Supplementary Discussion

1. The Observed Homo-associates are Located in the Plasma Membrane

One may be concerned whether the observed structures move indeed in the cellular plasma membrane or may represent cytosolic vesicles entering the field of view. We therefore performed several control experiments for both probes used in this study, i.e. mGFP-GPI and Bodipy-GM1.

- *mGFP is accessible from the extracellular milieu*: We tested, whether the mGFP is accessible to extracellular, non-membrane permeable reagents. First, we treated cells with phospholipase C (PLC), resulting in a reduction of the pixel brightness to ~17% (Supplemental Fig. 2); apparently, not all mGFP-GPI molecules were cleaved. However, the respective dimer fraction hardly changed indicating that the likelihood for cleavage of monomers or whole dimers was the same. Still, the remaining pool of ~40% dimers may still originate from cytosolic vesicles. We next applied the fluorescence quencher Trypan Blue, which further reduced the brightness to ~2.7%. The remaining population contains only a minute dimer fraction <10%. In summary, the mGFP is accessible from the extracellular milieu and thus unlikely to be located in cytosolic vesicles.

For Bodipy-GM1, the quenching and cleavage assays were unfeasible. Thus, for the lipid probe the following additional controls were performed.

- *The probes recover from the aperture edges*: Internalized Bodipy-GM1 would be associated with transport carriers that are actively transported along cytoskeletal filaments throughout the cytosol. Under non TIRF conditions we indeed frequently observed such active transport of very bright diffraction-limited spots, which could be easily identified. Under TIRF conditions, we did not observe such structures.

  However, vesicles carrying lower amounts of fluorescent lipid may be difficult to discriminate from membrane-associated probes, as in this case the brightness could be similar. Still, cytosolic vesicles can be discriminated from membrane bound probes due to their three-dimensional mobility: vesicles enter the photobleached region in general from the top, thereby traversing just the narrow evanescent field of ~100nm, whereas lateral diffusion of membrane constituents leads to a recovery from the edges of the photobleached region.

  We therefore analyzed the dimer fraction as function of the probe location within the photobleached area. Our rational was that vesicles should traverse the evanescent field

from the top and thus fill the photobleached region homogenously, whereas the membrane-anchored probes would recover from the edges of the photobleached area. In consequence, we would expect a higher dimer fraction in the central regions. However, for both Bodipy-GM1 and mGFP-GPI we did not observe any correlation between dimer fraction and probe location (Supplemental Fig. 2D & 2F).

- *There is no probe recovery at early time points:* We also tested whether signals appeared throughout the bleached area at earlier time-points, which would be indicative of vesicles attaching to the membrane from the cytosol. However, after a shorter recovery time of 50ms, we observed on average only about two Bodipy-GM1 spots in 10 images, which thus hardly affected the overall data sets (Supplemental Fig. 2E).
- *TOCCSL does not select for a minor fraction*: Since recovery from the top could be faster than the recovery within the membrane, one could argue that our TOCCSL technique selects for a hypothetical vesicular fraction. However, such vesicles should have a higher mobility than the membrane-bound probe. We therefore compared the Bodipy-GM1 mobilities obtained in the TOCCSL experiment with those obtained under low staining conditions without TOCCSL. Basically, the two approaches yielded identical diffusion constant values (TOCCSL: $D = 1.37 \pm 0.08$ μm^2/s versus low staining: $D = 1.35 \pm 0.16$ μm^2/s for Bodipy-GM1 in CHO cells at 37°C; see Supplemental Fig. 6).
- *All observed structures were traceable, irrespective of their brightness*: It is unlikely that cytosolic vesicles diffusing in three dimensions would stay within the evanescent field of ~100nm depth for at least three consecutive observations (our criterion for mobility analysis; it converts to a duration of 40ms): given the mobility, we estimate a time of only ~4ms to pass a distance of 100nm along the z-axis.
- *TOCCSL experiments under non-TIR excitation also yield Bodipy-GM1 homo-association*: We performed the TOCCSL experiments both under TIR and non-TIR excitation (Fig. 2 & Fig. 3, respectively). In both cases, we observed homo-association of Bodipy-GM1. Since conventional epi-illumination leads to a strong excitation and bleaching also of the cytosolic region above the focal plane, intracellular vesicles would be bleached and thus would hardly be included in the recovery image.

2. Additional Control Experiments to rule out Laser-induced Crosslinking

There are reports that photobleaching of chromophores may produce reactive oxygen species, which can be used for example to inactivate nearby proteins (1); additional side effects like protein crosslinking could be suspected. We therefore controlled whether the observed

mGFP-GPI association was artificially stabilized by the applied photobleaching pulse. In such a case, we would expect an accumulation of stable mGFP-GPI associates upon multiple photobleaching steps. However, we did not find an indication for an increase in α_2 (Supplemental Fig. 3B). The lack of artificial crosslinking is in agreement with a recent finding demonstrating that GFP is a rather ineffective chromophore for protein inactivation (2). Moreover, the inactivation range was reported to be limited to the immediate molecular neighborhood of the excited chromophore (1) so that mGFP-GPI associates located outside of the photobleached area should not be affected and thus the recovering dimers not photoinduced.

We further tested whether mGFP-GPI homo-associates in a model membrane that does not show phase separation. For this, we incorporated purified recombinant his-mGFP-GPI with the GPI-anchor sequence of the decay accelerating factor (DAF) into a supported DOPC bilayer. TOCCSL experiments revealed only a marginal dimer fraction of 1.2±0.9%, close to the detection limit of our method (Supplemental Fig. 4A). For comparison, we expressed the mGFP-GPI(DAF) in T24 cell and pooled cells with a similar surface density as achieved in the model membrane system (average σ=335 molecules/μm^2). We found a dimer fraction of 30±2.5% (Supplemental Fig. 4B) that is in accordance with the data obtained on CHO cells expressing mGFP-GPI(hFR) (Fig. 1E). Therefore, the mGFP-GPI does not dimerize in membranes *per se*. Note that the single molecule brightness was higher on the reconstituted system, presumably due to higher excitation intensity next to the glass surface.

3. Comparison of the Results with the Recent Literature

In the following, we give a survey over recent key experiments designed for studying plasma membrane rafts in living cells and discuss our data in relation to those results.

i) By determining the fluorescence anisotropy as a measure of homo-FRET, the group of Mayor showed in a series of papers that GPI-anchored proteins are distributed non-randomly in the live cell plasma membrane (3-5). Upon analyzing the dependence of the FRET signal on photobleaching and by fitting with a multi-parameter model, the authors concluded that the investigated proteins associate to small “nanoclusters” consisting of only up to 4 molecules (4). These clusters were distributed non-randomly in the plasma membrane, and concentrated to optically resolvable domains (3). From the photobleaching behavior, the presence of immobile nanoclusters was concluded. Our data on mGFP-GPI homo-association are in good quantitative agreement with

those experiments; in particular, both studies revealed a fraction of approximately one third of all mGFP-GPI proteins to be homo-associated within clusters (4). In contrast to Mayor's most recent paper (3), however, we found these structures to be freely mobile. The apparent discrepancy may be solved by noting that the two approaches are rather complementary: Mayor's technique is primarily sensitive to the detection of immobile structures, whereas our approach selects for mobile structures. It appears plausible that the two populations can interchange and therefore actually correspond to the same general pool.

ii) The group of Marguet introduced a new method based on FCS, in which the size of the laser-focus is varied (6, 7). Analyzing the diffusion time as function of the spot-size yields the so-called diffusion law, where positive offsets are regarded as indication for transient confinement to rafts. The method has been used and further improved by others, yielding consistent results (8, 9). The basic features of this approach can be summarized as follows: if the fluorescent probe would interact with immobile structures, the concomitant transient immobilization leads to a reduced diffusion constant, and – importantly – a positive offset in the diffusion law (10).
With this approach, cholesterol-dependent positive offsets in the diffusion law were indeed observed for GFP-GPI (6) and fluorescent sphingomyelin (8). As the offset originates from the transient trapping of the probe to small areas (<20nm in the case of Eggeling et al. (8)), the data indicate – similar to Mayor's experiments – the transient immobilization of the observed structures. Further conclusions on the mobile entities can hardly be drawn.

iii) There are a few reports on the association of raft proteins or lipids with larger domains (11-13). For example, Pinaud et al addressed the association behavior of GPI-anchored proteins with immobile GM1 patches induced by Cholera Toxin B. Association times in the order of tens of seconds were observed (13). Transient immobilization is a rather general phenomenon observed for membrane proteins, which typically leads to an immobile fraction in FRAP experiments. Taken together, we regard reversible immobilization of membrane platforms as the most plausible assumption to reconcile our data with the experiments discussed in i) and ii).

iv) A key paper on rafts originated from a collaboration from the Hörber and Simons group (14). In this work, large beads were coupled to individual membrane proteins and the local viscous drag was measured with a special optical tweezers arrangement. Since viscous drag reports the size of the diffusing object, Hörber et al were interested whether raft- and nonraft-proteins show different behavior, both under control conditions and upon depletion of cholesterol. Consistently, the raft markers yielded a lower drag upon cholesterol depletion, whereas no effect was observed for the nonraft proteins. In this study, local viscous drags were found to be constant over time scales of minutes, indicating that the associated rafts were rather long-lived, consistent with the data obtained in our study. A size of 26nm was estimated, using the Saffman-Delbrück relation for protein diffusion.

v) Results from single particle or single molecule tracking of plasma membrane constituents are frequently used to extract information on rafts. In particular, a review article published from the Kusumi lab can be tracked back to be the main source for the proposition of a short raft-lifetime of a millisecond or less (15), which would contrast our observation of stable structures. Kusumi's hypothesis was based on the picket-fence model of the plasma membrane developed by the group over years (16-20). By following the motion of gold-labeled proteins or lipids in the live cell plasma membrane, the researchers found hop diffusion between adjacent compartments induced by the underlying cortical actin meshwork. They postulated that actin-anchored proteins line up like pickets along the actin fences, thereby transmitting the structural information from the cytosolic to the exoplasmic leaflet of the lipid bilayer. In this model, the pickets would act like size-exclusion barriers to the motion of objects, thereby particularly limiting the transmission of rafts. Since raft markers (e.g. GPI-anchored proteins) showed the same hop frequency as non-rafts markers (e.g. the lipid dioleyl-phophatidylethanolamine (DOPE)), Kusumi et al. concluded that rafts have to be dissolved before the transit through the pickets, and therefore appear to be extremely short-lived. However, the effect of potential immobile and laterally arranged pickets on membrane rafts of unknown physical properties appears highly speculative.

In summary, a picture is emerging in which the plasma membrane contains protein assemblies that are stabilized by the lipid matrix; these platforms are reminiscent of lipid rafts as originally introduced by Simons and Ikonen (21):

1. The platforms are smaller than 30nm, and consequentially contain a limited set of cargo molecules.
2. The platforms confine their cargo over time scales of seconds.
3. The integrity of the platforms depends on the presence of cholesterol
4. A significant fraction of platforms is freely diffusing in the plasma membrane. Transient immobilization by interaction with static structures can be expected to occur.
5. Homo-association of proteins in the platforms may change upon alterations of the environmental conditions (shown in this study for elevated temperature).

Supplementary Materials & Methods

1. Fusion Constructs & Cell Culture

The GFP of this vector was mutated at amino acid position 206 from alanine to lysine to get a monomeric GFP (mGFP) variant (22). CHO cells (ATTC # CCL-61) were stably transfected and cultured in DMEM/HAMS-F12 (PAA-Laboratories, Pasching, Austria) supplemented with 5% fetal calf serum (PAA-Laboratories) and 400µg/ml neomycin (G418, PAA-Laboratories). Jurkat T-cells (clone E6.1, ATTC # TIB-152) were cultured in RPMI 1640 medium (PAA-Laboratories) supplemented with 10% fetal calf serum. T24 cells (DSMZ # ACC 310) were stably transfected with mGFP-GPI(DAF) (23) (a kind gift by Daniel Legler, University of Konstanz) and cultured in RPMI 1640 medium (PAA-Laboratories) supplemented with 10% fetal calf serum (PAA-Laboratories) and 400µg/ml neomycin (G418, PAA-Laboratories). All cell lines were incubated at 37°C in a 5% CO2 atmosphere.

Confluent CHO and T24 cells were harvested using trypsin/EDTA (PAA-Laboratories) and seeded onto 30mm glass slides (#1, Menzel, Braunschweig, Germany) in Petri-dishes at least 24 hours before experiments.

2. Separation of detergent resistant membrane microdomains by sucrose-gradient centrifugation.

Detergent resistant microdomain separation was performed as described previously (24). Briefly, cells (2.5×10^7) were lysed for 30 min at 4°C in ice-cold lysis buffer [20 mM Tris/HCl (pH 7.5), 150mM NaCl and „complete“ protease inhibitor cocktail (Roche)

containing 1% Brij-58 (Pierce, Rockford, IL)]. Cell lysate was adjusted to 40% (wt/vol) sucrose by adding an equal volume of an 80% sucrose solution (TBS containing 80% wt/vol sucrose and protease inhibitors). These preparations were placed in an ultracentrifuge tube (Sorvall Instruments-Du Pont, Wilmington, DE). On top of this, layers of 30% and 5% sucrose were placed. After ultracentrifugation (180,000 g, 16 h, 4°C), 500 µl fractions were collected from the top. Aliquots of each fraction were diluted in a 4x gel loading SDS-buffer. Proteins were separated by SDS-PAGE, immunoblotted followed by probing the membranes with anti-GFP mAb clone B2 (Santa Cruz Biotechnology, Santa Cruz, CA).

3. Flow cytometric assay of detergent resistance (FCDR)

The assay was carried out as described previously (25). $5x10^5$ Jurkat cells expressing mGFP-GPI were applied per sample. Non-specific binding sites on the cell surface were blocked by incubation with 2% (w/v) human IgG (Beriglobin) for 20min on ice. The cells were stained with the mouse anti-GFP mAb 11E5 (IgG1, purchased from Invitrogen), mAb MEM-189 to CD71 (IgG1), mAb MEM-102 to CD48 (IgG1), or mAb MEM-43 to CD59 (IgG2a), all kind gifts from Vaclav Horejsi, Institute of Molecular Genetics, Academy of Sciences of the Czech Republic, Prague, Czech Republic. The mAbs were used with 10µg/ml final concentration and an incubation time of 30min on ice. After a subsequent washing step, the primary antibodies were detected with an allophycocyanin (APC)-conjugated AffiniPure F(ab')2 goat anti-mouse IgG+IgM (H+L) fragment (Jackson ImmunoResearch Laboratories, Inc.) applied in a 1:100 dilution for 30min on ice. After washing, the cells were resuspended in PBS and the fluorescence intensities were recorded with an LSRII flow cytometer (Becton-Dickinson, San Jose, CA, USA). Then the remaining cells were pelleted (350 x g, 3 min, 4°C), resuspended in ice-cold 0.1% (w/v) Triton X-100 (Pierce/Thermo Fisher Scientific), and after an incubation period of 5 min on ice, the fluorescence signals were immediately measured with the flow cytometer. Data collection and analysis were performed by FACSDiva (Becton-Dickinson) and FlowJo (Tree Star, Inc. Ashland, OR, USA) softwares, respectively.

FCDR was evaluated according to the following equation: $FCDR = (FL_{det} - FLBg_{det})/(FL_{max} - FLBg)$, where FL_{max} is the mean fluorescence intensity (MFI) of the labeled untreated cells, FL_{det} is the MFI of the labeled cells treated with the detergent, FLBg and $FLBg_{det}$ are the MFIs of autofluorescence of the isotype control-labeled cells before and after detergent treatment, respectively. An FCDR index of 1.00 means complete detergent resistance whereas an FCDR index of 0.00 means complete sensitivity.

4. Sample Preparation

Jurkat cells with passage numbers 8-16 were centrifuged for 3min at 2000rpm and 4°C. The pellet was resuspended in 30µl HBSS containing Bodipy-GM1 with concentrations ranging from 1µM to 2.5µM and incubated for 30min at 4°C. Two centrifugation steps removed the unbound marker. Cells were resuspended in HBSS and stored at 4°C to avoid endocytosis of Bodipy-GM1. In some cases, Lab-Tek chambered coverglass (# 155411, Nunc, Thermo Fisher Scientific, Rochester, NY) was incubated for 1h at 37°C with 0.01% Poly-L-Lysine (#P1399, Sigma-Aldrich, St. Louis, MO) dissolved in Dulbecco's Phosphate Buffered Saline (PBS, PAA-Laboratories). We observed no effect of Poly-L-Lysine treatment on the data. After two washing steps, 5-10µl of the cell suspension was added to the chamber. Experiments were performed in HBSS at 37°C except were indicated.

5. Supported Lipid Bilayer Preparation

1,2-Dioleoyl-sn-glycero-3-phosphocholine (DOPC, Avanti Polar Lipids, Alabaster, AL) was diluted in PBS and mixed with purified his-mGFP-GPI(DAF) yielding final concentrations of 10mg/ml and 40µg/ml, respectively. Vesicles were formed via sonification in a water bath for 10min at room temperature. Piranha cleaned glass coverslips (Menzel #1, Braunschweig, Germany) were glued to the measurement chamber (Lab-Tek, NUNC) from which the bottom glass slide was removed. The vesicle solution was diluted 1:3 in PBS and the bilayer was formed from this solution through self-assembly on glass coverslips. After 20min at room temperature the bilayer was rinsed thoroughly with PBS and TOCCSL experiments were performed as described in section 1.5.

6. Western Blotting

The protein concentration was measured by using the Bio-Rad RC DC protein assay. Cell lysate aliquots corresponding to 20 µg of protein were separated on 12% SDS gels and then transferred to PVDF membranes. The membranes were probed with anti-Hsp70, anti-Hsp27 (SPA-810; SPA-803, respectively, both Stressgen, Ann Arbor, MI) or anti-actin (A5060, Sigma-Aldrich) antibodies. The antibody-recognized molecules were visualized by using HRP conjugated secondary antibodies and the Millipore Immobilon Chemiluminescent HRP substrate (Millipore, Billerica, MA). Quantification of the bands was done by the AlphaImager HP System (Alpha Innotech, San Leandro, CA).

7. Microscopy

A Zeiss Axiovert 200 microscope was equipped with a 100x NA=1.46 α Plan - APOCHROMAT objective (Zeiss, Oberkochen Germany). Samples were illuminated in objective-based total internal reflection (TIR) configuration via the epiport using 488nm light from an Ar^+ Laser (Model 2017-05AR, Spectra Physics, Mountain View, CA) with an intensity of typically 9-11 kW/cm^2. A slit aperture (Zeiss) with a width of ~7µm in the object plane was used as field stop to confine the illumination area. After appropriate filtering (HQ535/50 and 505DCLP, Chroma, Rockingham, Vt) to effectively block Rayleigh scattered light, fluorescence images were recorded using a back-illuminated nitrogen cooled CCD camera (Micro Max 1300-PB, Roper Scientific, Tucson, AZ).

8. Data Analysis

Trajectories are specified by a sequence of positions $\vec{x}(i)$, with i ranging from 1 to the number of observations of this trajectory. The mean square displacements $\left\langle r^2 \right\rangle$ were calculated as a function of the time-lag $t_{lag} = n(t_{ill} + t_{del})$ according to $\left\langle r^2 \right\rangle = \left\langle (\vec{x}(i) - \vec{x}(i+n))^2 \right\rangle_{i=1,1+n,1+2n,\ldots}$ with n denoting the difference in frame index. Data were analyzed by fitting with the function $\left\langle r^2 \right\rangle = 4Dt_{lag} + 4\sigma_{xy}^2$, yielding the lateral diffusion constant D and the single molecule localization precision σ_{xy} (26). We further analyzed each trajectory separately by calculating an estimator of the single spot mobility according to $D_{spot} = \left\langle \frac{r^2(t_{lag})}{4t_{lag}} \right\rangle$.

Single molecule brightness analysis was performed as described previously (27, 28). Due to the stochastic emission process, the number of photons, *B*, detected from a single dye molecule is characterized by the probability density function $\rho_1(B)$. Therefore, $\rho_1(B)dB$ denotes the probability that an intensity measurement reveals a number of detected photons within the interval $[B, B + dB]$. The corresponding intensity distribution of *N* colocalized independent emitters, $\rho_N(B)$, can be calculated recursively as a series of convolution integrals $\rho_N(B) = \int \rho_1(B')\rho_{N-1}(B - B')dB'$. Consequentially, the average brightness of two homo-associated molecules would be twice the monomer brightness; this was previously confirmed for enhanced GFP (29). Given a mixed population of monomers and various types

of oligomers, the resulting intensity distribution is given by a linear combination of these different distributions

$$\rho(B) = \sum_{N=1}^{N_{max}} \alpha_N \cdot \rho_N(B) \qquad \text{Eq. S1}$$

The weights of the individual distributions, α_N, with $\sum_{N=1}^{N_{max}} \alpha_N = 1$ correspond to the fractions of the respective N-mers present. Experiments were based on measuring $\rho(B)$ and $\rho_1(B)$; the weights α_N were determined by non-linear least squares fitting. A Bayesian probability update was used to determine the error-bars for α_2 (30).

References

1. Tanabe T, *et al.* (2005) Multiphoton excitation-evoked chromophore-assisted laser inactivation using green fluorescent protein. *Nat Methods* 2(7):503-505.
2. Tour O, Meijer RM, Zacharias DA, Adams SR, & Tsien RY (2003) Genetically targeted chromophore-assisted light inactivation. *Nat Biotechnol* 21(12):1505-1508.
3. Goswami D, *et al.* (2008) Nanoclusters of GPI-anchored proteins are formed by cortical actin-driven activity. *Cell* 135(6):1085-1097.
4. Sharma P, *et al.* (2004) Nanoscale Organization of Multiple GPI-Anchored Proteins in Living Cell Membranes. *Cell* 116(4):577-589.
5. Varma R & Mayor S (1998) GPI-anchored proteins are organized in submicron domains at the cell surface. *Nature* 394(6695):798-801.
6. Lenne PF, *et al.* (2006) Dynamic molecular confinement in the plasma membrane by microdomains and the cytoskeleton meshwork. *Embo J* 25(14):3245-3256.
7. Wawrezinieck L, Rigneault H, Marguet D, & Lenne PF (2005) Fluorescence correlation spectroscopy diffusion laws to probe the submicron cell membrane organization. *Biophys J* 89(6):4029-4042.
8. Eggeling C, *et al.* (2008) Direct observation of the nanoscale dynamics of membrane lipids in a living cell. *Nature* 457:1159-1162.
9. Humpolikova J, *et al.* (2006) Probing diffusion laws within cellular membranes by Z-scan fluorescence correlation spectroscopy. *Biophys J* 91(3):L23-L25.
10. Ringemann C, *et al.* (2009) Exploring single-molecule dynamics with fluorescence nanoscopy. *New Journal of Physics* 11:103054.
11. Hess ST, *et al.* (2007) Dynamic clustered distribution of hemagglutinin resolved at 40 nm in living cell membranes discriminates between raft theories. *Proc Natl Acad Sci U S A* 104(44):17370-17375.
12. Schütz GJ, Kada G, Pastushenko VP, & Schindler H (2000) Properties of lipid microdomains in a muscle cell membrane visualized by single molecule microscopy. *Embo J* 19(5):892-901.
13. Pinaud F, *et al.* (2009) Dynamic Partitioning of a Glycosyl-Phosphatidylinositol-Anchored Protein in Glycosphingolipid-Rich Microdomains Imaged by Single-Quantum Dot Tracking. *Traffic* 10(6):691-712.
14. Pralle A, Keller P, Florin EL, Simons K, & Horber JK (2000) Sphingolipid-cholesterol rafts diffuse as small entities in the plasma membrane of mammalian cells. *J Cell Biol* 148(5):997-1008.

15. Kusumi A, Koyama-Honda I, & Suzuki K (2004) Molecular dynamics and interactions for creation of stimulation-induced stabilized rafts from small unstable steady-state rafts. *Traffic* 5(4):213-230.
16. Fujiwara T, Ritchie K, Murakoshi H, Jacobson K, & Kusumi A (2002) Phospholipids undergo hop diffusion in compartmentalized cell membrane. *J Cell Biol* 157(6):1071-1081.
17. Murase K, *et al.* (2004) Ultrafine Membrane Compartments for Molecular Diffusion as Revealed by Single Molecule Techniques. *Biophys J* 86(6):4075-4093.
18. Suzuki K, Ritchie K, Kajikawa E, Fujiwara T, & Kusumi A (2005) Rapid hop diffusion of a G-protein-coupled receptor in the plasma membrane as revealed by single-molecule techniques. *Biophys J* 88(5):3659-3680.
19. Umemura YM, *et al.* (2008) Both MHC class II and its GPI-anchored form undergo hop diffusion as observed by single-molecule tracking. *Biophys J* 95:435-450.
20. Kusumi A, *et al.* (2005) Paradigm shift of the plasma membrane concept from the two-dimensional continuum fluid to the partitioned fluid: high-speed single-molecule tracking of membrane molecules. *Annu Rev Biophys Biomol Struct* 34:351-378.
21. Simons K & Ikonen E (1997) Functional rafts in cell membranes. *Nature* 387(6633):569-572.
22. Zacharias DA, Violin JD, Newton AC, & Tsien RY (2002) Partitioning of lipid-modified monomeric GFPs into membrane microdomains of live cells. *Science* 296(5569):913-916.
23. Legler DF, *et al.* (2005) Differential insertion of GPI-anchored GFPs into lipid rafts of live cells. *Faseb J* 19(1):73-75.
24. Muhammad A, *et al.* (2009) Sequential cooperation of CD2 and CD48 in the buildup of the early TCR signalosome. *J Immunol* 182(12):7672-7680.
25. Gombos I, *et al.* (2004) Cholesterol sensitivity of detergent resistance: a rapid flow cytometric test for detecting constitutive or induced raft association of membrane proteins. *Cytometry A* 61(2):117-126.
26. Wieser S, Moertelmaier M, Fuertbauer E, Stockinger H, & Schütz GJ (2007) (Un)Confined Diffusion of CD59 in the Plasma Membrane Determined by High-Resolution Single Molecule Microscopy. *Biophys J* 92(10):3719-3728.
27. Schmidt T, Schütz GJ, Gruber HJ, & Schindler H (1996) Local stoichiometries determined by counting individual molecules. *Anal Chem* 68(24):4397-4401.
28. Moertelmaier M, Brameshuber M, Linimeier M, Schütz GJ, & Stockinger H (2005) Thinning out clusters while conserving stoichiometry of labeling. *Appl Phys Lett* 87:263903.
29. Chen Y, Wei LN, & Muller JD (2003) Probing protein oligomerization in living cells with fluorescence fluctuation spectroscopy. *Proc Natl Acad Sci U S A* 100(26):15492-15497.
30. Bolstad WM (2007) *Introduction to Bayesian statistics* (Wiley Interscience, Hoboken, NJ) second edition Ed.

Supplemental Figures 1-7

Supplemental Fig. 1

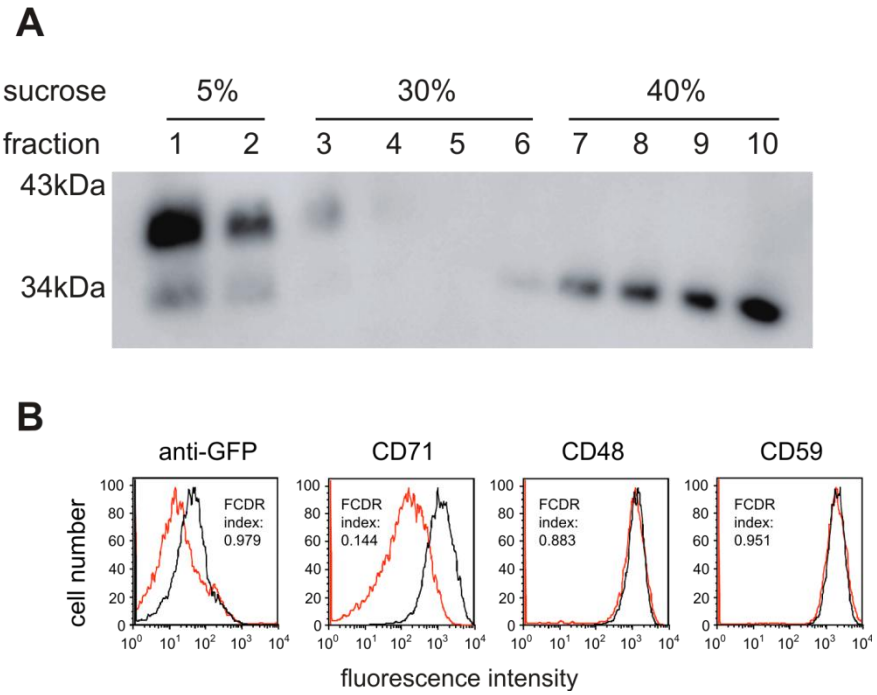

Supplemental Fig. 1. Lipid raft partitioning of mGFP-GPI in CHO and Jurkat T cells. (A) CHO cells transfected with mGFP-GPI were lysed in a buffer containing the nonionic detergent Brij-58 (1%) and lipid raft partitioning was analyzed by sucrose gradient ultracentrifugation and immunoblotting using the anti-GFP mAb clone B2. (B) Flow cytometric assay of detergent resistance (FCDR). Because of the very low expression level of mGFP-GPI in Jurkat T cells, we were unable to detect the protein by immunoblotting. Therefore, we decided to apply immunofluorescent labeling of mGFP-GPI on the cell surface and test its resistance/sensitivity to the non-ionic detergent Triton X-100 using a flow cytometric assay. Jurkat T cells expressing mGFP-GPI were surface-labeled with either an anti-GFP mAb, or an mAb to CD71 (non-raft protein, negative control), or CD48, CD59 (raft-associated GPI-proteins, positive controls). The primary mAbs were visualized by an APC-conjugated secondary anti-mouse reagent. Histograms show fluorescence intensity distribution of the samples before (black line) and after treatment with ice-cold 0.1% (w/v) Triton X-100 for 5min on ice (red line). Flow cytometric detergent resistance (FCDR) indices are also shown.

Supplemental Fig. 2

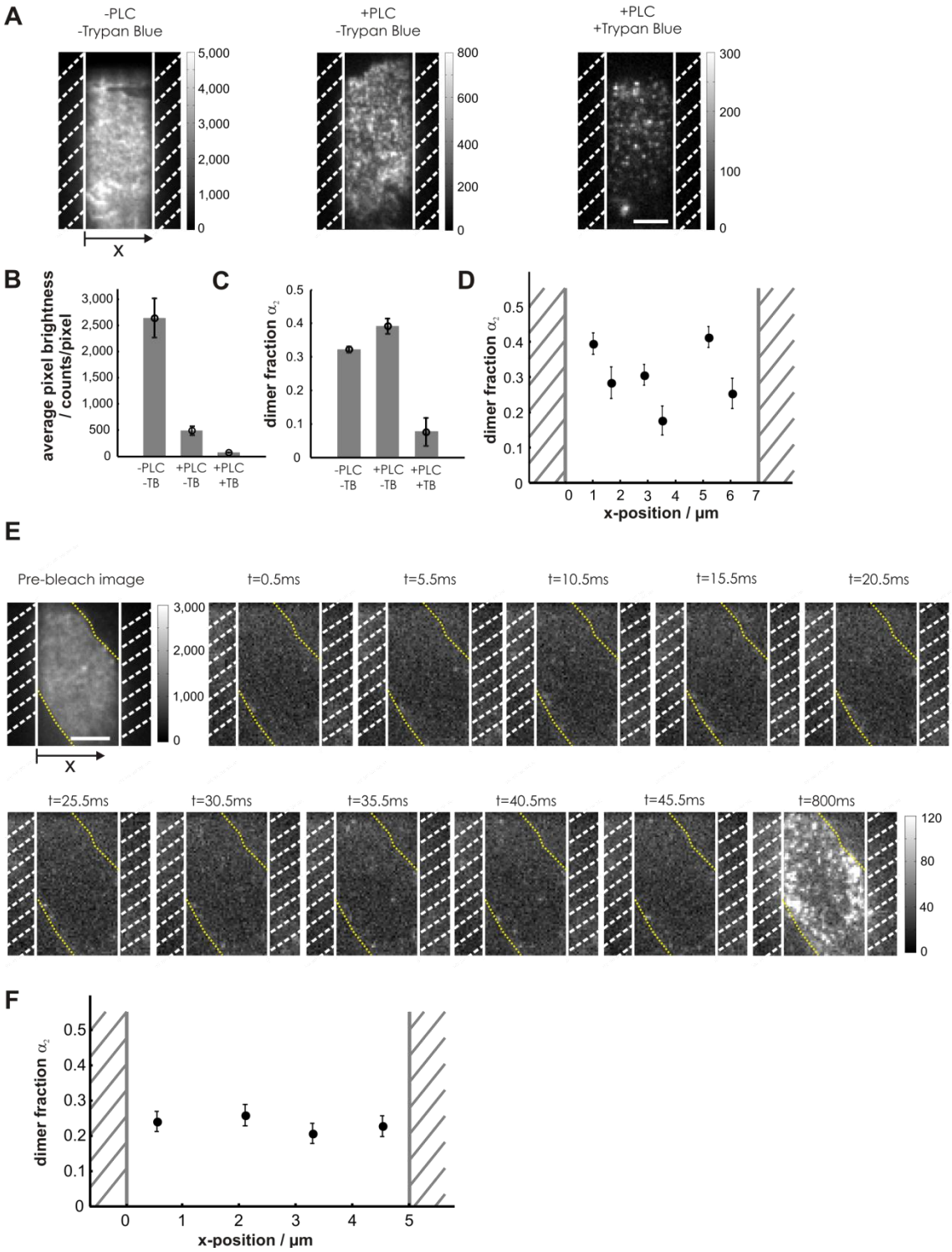

Supplemental Fig. 2. Control experiments to rule out the contribution of cytosolic mGFP-GPI or Bodipy-GM1 positive vesicles. (A) Pre-bleach images of mGFP-GPI expressing CHO cells before treatment (left), after cleavage of the GPI-anchor with PLC (middle) and after additional mGFP quenching with Trypan Blue. Grey scales were adjusted for all images separately, and indicated in the bar to facilitate comparison. Imaging conditions were identical, therefore the arbitrary units are comparable. Scale bar 4µm. (B) shows the average

pixel brightness of several cells after the described treatment, (C) the according dimer fraction. (D) The dimer fraction was analyzed as a function of the spatial coordinate within the field of view as indicated in A. For this, data were sorted according to the x-position and pooled in subsets of equal size. The aperture is indicated as hashed area. (E) A cell is shown before the bleaching pulse, and at defined timings after photobleaching. To guide the eye, the cell contour obtained in the pre-bleach image was indicated in the post-bleach images as yellow line. Grey scales were changed between the pre-bleach and the post-bleach images, and are indicated as bars. Within the first 50ms after the bleaching pulse we observed hardly any spots. For comparison, we also provide a standard TOCCSL image recorded after a recovery time of 800ms. Scale bar 4µm. (F) The Bodipy-GM1 dimer fraction was analyzed as a function of the spatial coordinate within the field of view. For this, standard TOCCSL experiments performed at t_{rec}=800ms or t_{rec}=1400ms were included. Data were sorted according to the x-position and pooled in subsets of equal size. The aperture is indicated as hashed area. All experiments were performed at 37°C.

Supplemental Fig. 3

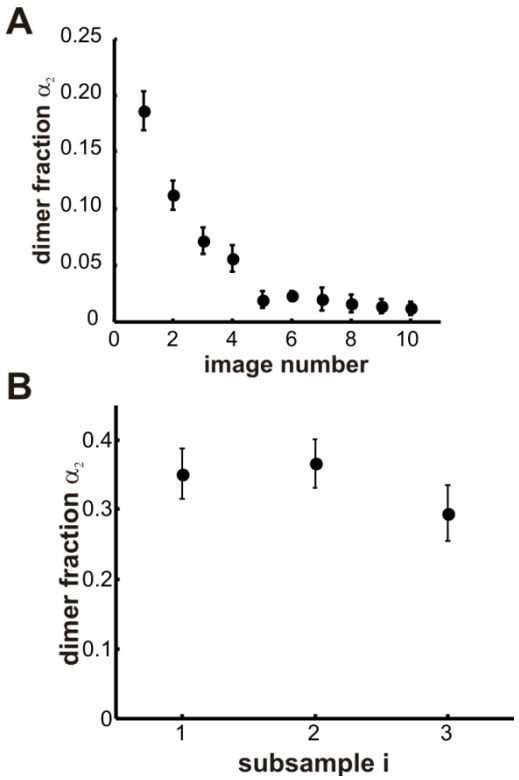

Supplemental Fig. 3. Additional control experiments. (A) The dimer fraction was determined as a function of the image number within trajectories. The dimer fraction decreases due to photobleaching, yielding essentially no dimers after the fifth observation. All experiments were performed at 37°C. (B) Control for photoinduced crosslinking. We tested whether running consecutive experiments on the same cells affects the results. For this, we recorded 60 consecutive TOCCSL runs on the same cell, and split the data into 3 successive subsamples of 20 runs for analysis. The experiment was repeated on 14 cells, and the individual subsamples were averaged. An exponential increase $\alpha_2 = 1 - \exp(k \cdot i)$ would characterize the generation of photo-crosslinking products; in this equation, i numbers the subsample and $k = \log[1 - \alpha_2(i = 1)]$ denotes the rate-constant. However, we did not find any indication for an increase in α_2. The experiments were performed at 37°C.

Supplemental Fig. 4

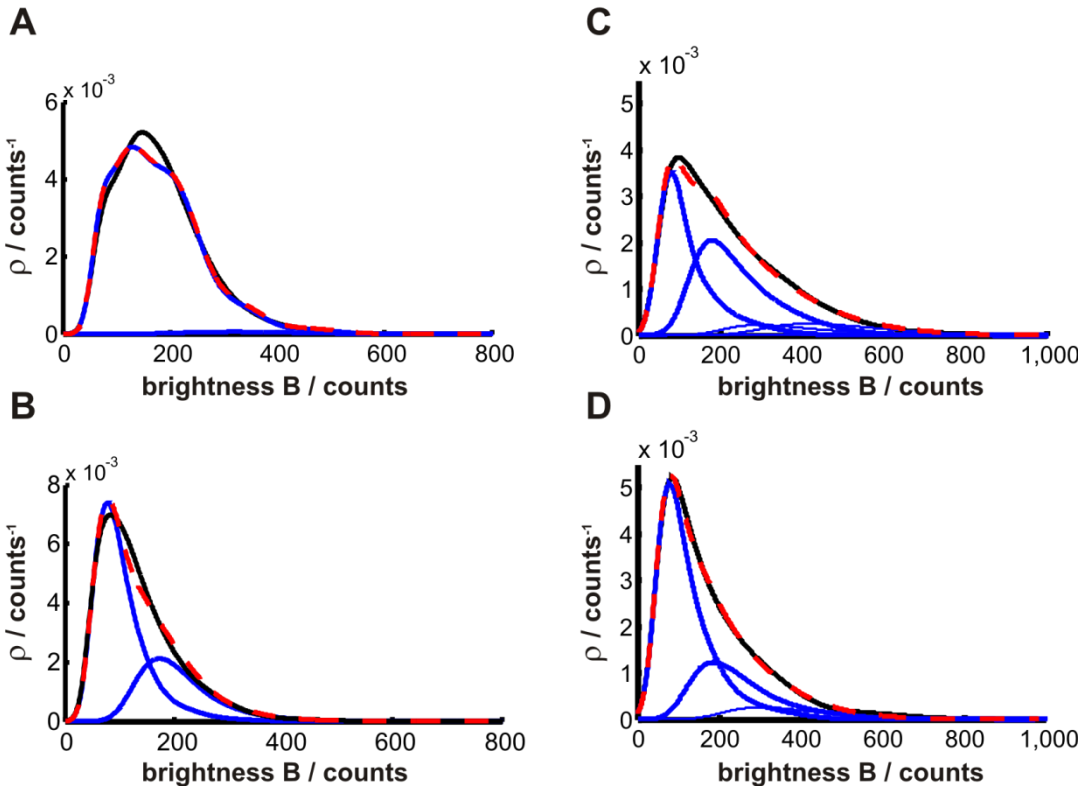

Supplemental Fig. 4. (A+B) Reconstitution in a model membrane. (A) his-mGFP-GPI(DAF) was purified and incorporated in a fluid supported DOPC bilayer at a surface density σ=180 molecules/μm^2. TOCCSL experiments revealed a dimer fraction of only 1.2±0.9%. (B) For comparison, we expressed mGFP-GPI(DAF) in T24 cells and recorded the degree of homo-association. Cells with a low surface density were pooled (σ=335 molecules/μm^2) yielding a dimer fraction of 30±2.5. (C+D) mGFP-GPI homo-association on Jurkat T cells. The brightness distributions of single mGFP-GPI spots in Jurkat T cells without (C) and after cholesterol depletion with COase (D) are plotted as probability density functions. Experiments were performed at 37°C. Data (black line) were fitted by Eq. S1 (red line); blue lines indicate monomer, dimer and higher order contributions. The fit yielded α_1=0.42, α_2=0.43, α_3=0.06, α_4=0.09 for (C), and α_1=0.65, α_2=0.29, α_3=0.06, α_4=0.00 for (D). The probe surface density was σ=109±12 μm^{-2} (C) and σ=124±11 μm^{-2} (D).

Supplemental Fig. 5

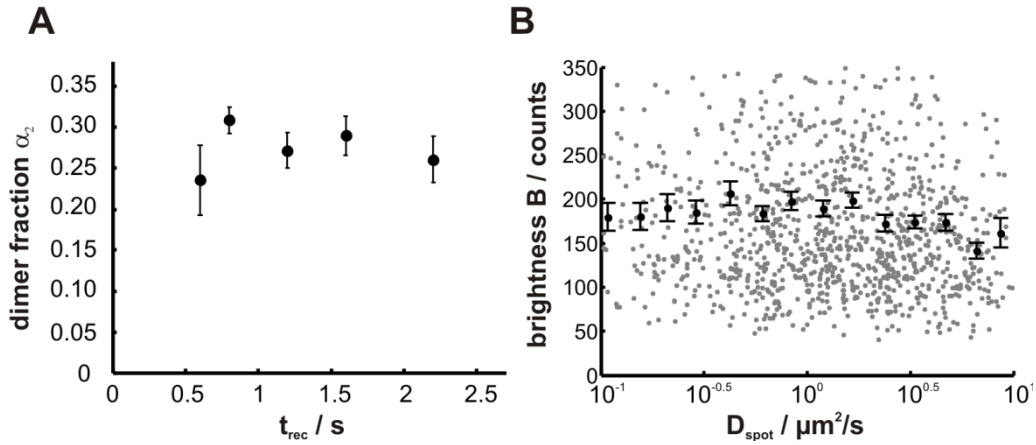

Supplemental Fig. 5. Dynamical behavior of mGFP-GPI clusters in CHO cells. Dynamical behavior of mGFP-GPI clusters in CHO cells. (A) The lifetime of clusters was assessed by determining the dependence of the dimer fraction α_2 on the recovery time t_{rec}. Up to 2.2s we found no significant correlation (*corr* = 0.037), indicating that clusters are stable on a seconds time-scale. (B) Correlation analysis of single spot brightness *B* and mobility D_{spot} (grey points). To facilitate the reading of the figure, we also provide the mean value of brightness and mobility in equally spaced bins along the x-axis (black points). No significant correlation was observed (*corr* = -0.085). Experiments were performed at 37°C.

Supplemental Fig. 6

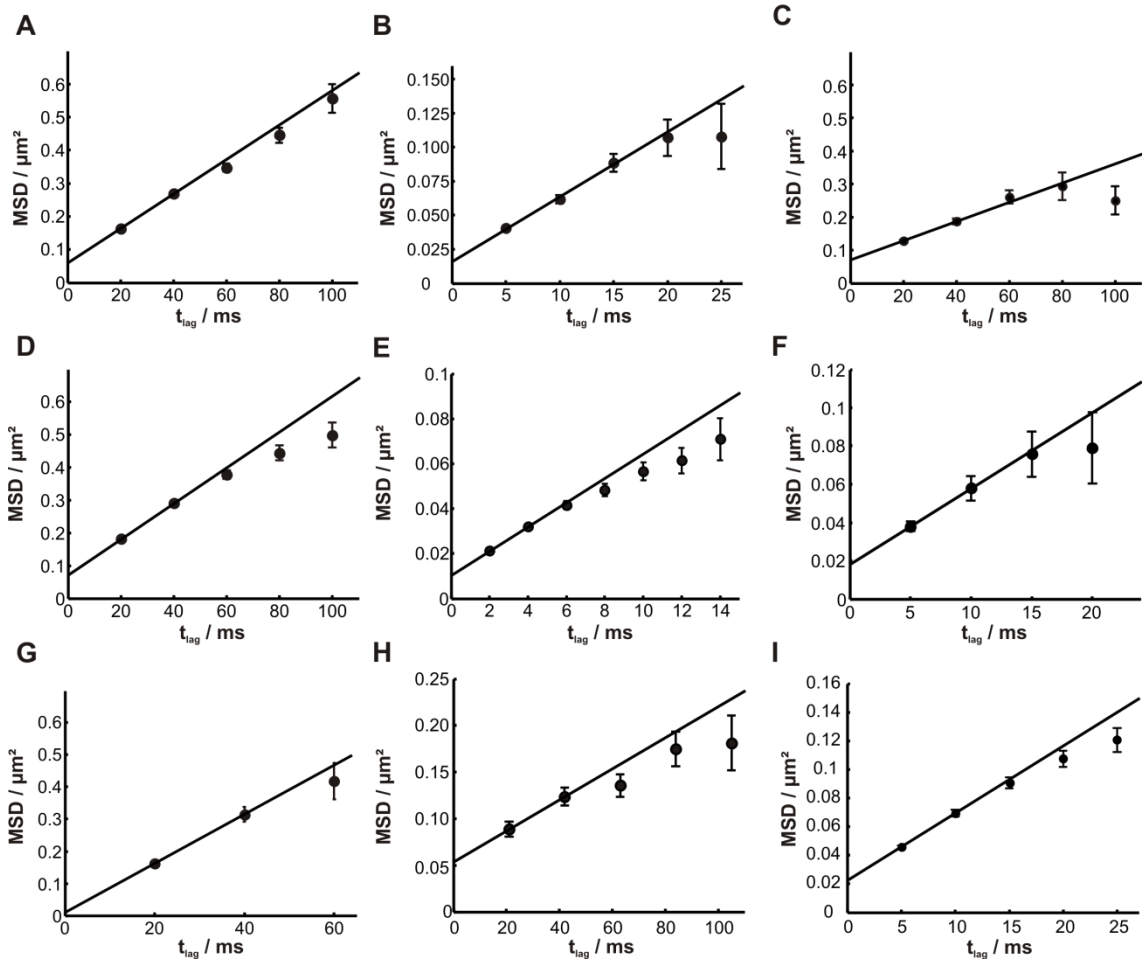

Supplemental Fig. 6. Mobility analysis. MSD is shown as function of t_{lag}; diffusion constants were determined by fitting with the function $MSD = 4Dt_{lag} + 4\sigma_{xy}^2$. Only the first two data points were considered for the fits. All data were obtained from the TOCCSL images unless denoted. The following experiments were performed: (A) mGFP-GPI on CHO cells at 37°C (D = 1.30 ± 0.08 µm^2/s); (B) mGFP-GPI on CHO cells at 37°C recorded in standard single molecule tracking after extensive photobleaching (D = 1.20 ± 0.17 µm^2/s); (C) mGFP-GPI on CHO cells at 37°C after cholesterol extraction using COase (D = 0.73 ± 0.11µm^2/s); (D) Bodipy-GM1 on CHO cells at 37°C (D = 1.37 ± 0.08 µm^2/s); (E) Bodipy-GM1 on CHO cells at 37°C recorded in standard single molecule tracking experiments using a low concentration of Bodipy-GM1 (D = 1.35 ± 0.16 µm^2/s); (F) mGFP-GPI on Jurkat T cells at 37°C (D = 0.99 ± 0.3µm^2/s), (G) Bodipy-GM1 on Jurkat T cells at 37°C (D = 1.91 ± 0.16µm^2/s); (H) Bodipy-GM1 on Jurkat T cells at 25°C (D = 0.42 ± 0.16µm^2/s); (I) Bodipy-GM1 on CHO cells at 37°C after cholesterol extraction and replenishment using MβCD (D=1.18 ± 0.12µm^2/s).

Supplemental Fig. 7

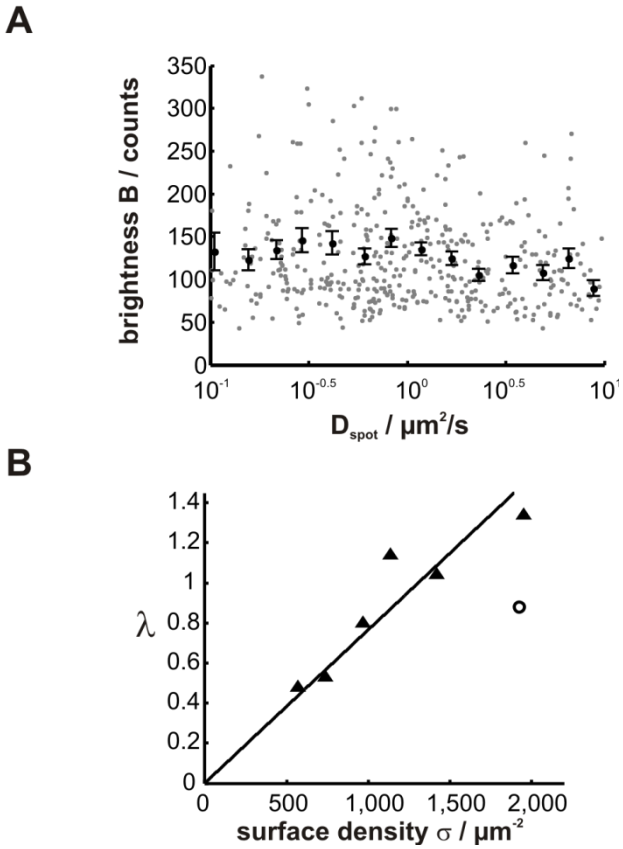

Supplemental Fig. 7. (A) Correlation analysis for brightness versus mobility. Correlation analysis of single spot brightness and mobility D_{spot} (grey points) for mGFP-GPI on cholesterol-depleted CHO cells at 37°C. To facilitate the reading of the figure, we also provide the mean value of brightness and mobility in equally spaced bins along the x-axis (black points). No significant correlation was observed (*corr* = -0.089). (B) Cholesterol-dependence of Bodipy-GM1 homo-association on Jurkat T cells at 25°C. Cholesterol-dependence of Bodipy-GM1 homo-association on Jurkat T cells at 25°C. The plot contains the same data as Fig. 3C, but further includes measurements after cholesterol extraction using MβCD (open circle). The fit parameter λ is plotted as a function of the surface staining σ (triangles). The applied MβCD concentration was here not sufficient to fully disrupt rafts, yet the cholesterol-dependence is confirmed by the significant decrease in λ.

Supplemental Table 1: Results from mobility analysis

probe molecule	cell type	T	mobile fraction	D (μm²/s)
mGFP-GPI	CHO	37°C	0.76 ± 0.05	1.30 ± 0.08
mGFP-GPI	CHO (depl. Cholesterol)	37°C	0.68 ± 0.10	0.73 ± 0.11
mGFP-GPI	Jurkat	37°C	0.92 ± 0.06	0.99 ± 0.3
Bodipy-GM1	CHO	37°C	0.67 ± 0.06	1.37 ± 0.08
Bodipy-GM1	CHO (depl. Cholesterol)	37°C	0.54 ± 0.11	N.D.
Bodipy-GM1	CHO (depl. and replenished Cholesterol)	37°C	N.D.	1.18 ± 0.12
Bodipy-GM1	Jurkat	37°C	0.60 ± 0.02	1.91 ± 0.16
Bodipy-GM1	Jurkat (depl. Cholesterol)	37°C	0.58 ± 0.05	N.D.
Bodipy-GM1	Jurkat	25°C	0.65 ± 0.12	0.42 ± 0.16
Bodipy-GM1	Jurkat (depl. Cholesterol)	25°C	0.64 ± 0.11	N.D.

Supplemental Table 1. The table shows the mobile fraction and the diffusion constant D for probes, cells and temperatures specified (mean ± s.e.m.) under normal conditions or upon cholesterol depletion / replenishment.

Supplemental Table 2: Information on sample sizes.

	# of spots or traces*	# of cells
Fig. 1E	2,464	14
Fig. 1F	672	9
Fig. 1G	1,238	8
Fig. 1H, COase treatment	443	6
Fig. 2A, full black circles	5,410	14
Fig. 2A, open red triangles	1,073	3
Fig. 2A, full red circle	754	5
Fig. 2A, open black circle	1,702	5
Fig. 2B, full circles	13,120	15
Fig. 2B, open red triangle	1,290	4
Fig. 3B, from the top	248	3
	299	5
	314	5
	148	6
	334	6
	1,321	5
Fig. 4 @ 37°C	2,464	14
Fig. 4 @ 39°C	419	6
Fig. 4 @ 41°C	663	7
Supplemental Fig. 2C –PLC-TB	2,464	14
Supplemental Fig. 2C +PLC-TB	1,107	5
Supplemental Fig. 2C +PLC+TB	280	6
Supplemental Fig. 2D	2,522	14
Supplemental Fig. 2F	1,561	5
Supplemental Fig. 3A	14,933	10
Supplemental Fig. 3B	2,464	14
Supplemental Fig. 4A	344	n.a.
Supplemental Fig. 4B	790	5
Supplemental Fig. 4C	1,011	7
Supplemental Fig. 4D	693	12
Supplemental Fig. 5A	2,464	14
Supplemental Fig. 5B	1,139*	16
Supplemental Fig. 6A	4,640*	14
Supplemental Fig. 6B	1,580*	3
Supplemental Fig. 6C	2,057*	6
Supplemental Fig. 6D	6,216*	12
Supplemental Fig. 6E	2,075*	3
Supplemental Fig. 6F	663*	7
Supplemental Fig. 6G	356*	3
Supplemental Fig. 6H	479*	18
Supplemental Fig. 6I	3,122*	4
Supplemental Fig. 7A	438*	6
Supplemental Fig. 7B (open symbol)	1,001	7